ACS Photonics

pubs.acs.org/journal/apchd5

Article

Voltage-Tunable Multifunctional Zoom Imaging Metalenses

Melissa Bosch,* Maxim Shcherbakov, Kanghee Won, Hong-Seok Lee, Young Kim, and Gennady Shvets*

Cite This: https://doi.org/10.1021/acsphotonics.4c01530

Read Online

ACCESS | Metrics & More | Article Recommendations | Supporting Information

ABSTRACT: Many contemporary imaging systems seek tunable focusing components with minimal form factors and versatile functionalities; however, existing solutions are typically limited in size, efficiency, and tuning speed. Here, low-loss all-dielectric metasurfaces integrated with liquid crystals (LCs) are used to demonstrate highly compact multifunctional zoom components. The phase profiles imparted by the metalens are modulated in real time by means of field-dependent LCs, enabling electrically driven continuous focal length variation and active bifocal imaging with low applied voltages (<10 V). These applications are achieved through the systematic design and validation of resonant metasurface elements that ensure the desired metalens response in each LC state. We engineer and fabricate a high-contrast voltage-actuated continuous-zoom LC-metalens with up to 18% total shift in focal length. Additionally, we fabricate simplified large-diameter LC-metalenses, composed of only a few resonator types, that facilitate electrically tunable multidepth imaging. These results demonstrate the promise of electrically controlled LC-embedded zoom-metasurfaces to serve as lightweight and ultrathin multifunctional focusing components, with prospective uses in next-generation imaging devices.

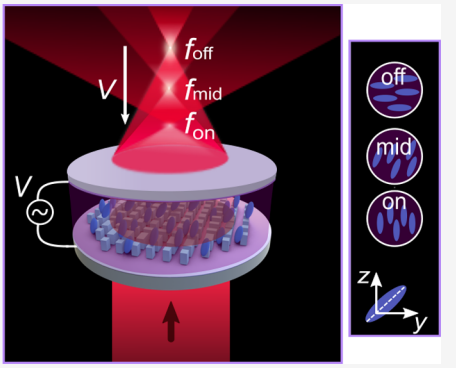

KEYWORDS: *varifocal lenses, metasurfaces, liquid crystals, imaging, nanofabrication*

INTRODUCTION

Zoom lenses with reconfigurable focal lengths are universal components of optical imaging and sensing technologies. Modern imaging systems with highly compact forms, such as mobile cameras, adaptive vision devices, and wearable mixed-reality displays, motivate the development of new miniature multifunctional zoom lens architectures. Traditionally, adjusting the focal length of a lens has relied on the mechanical translation of freeform refractive optical components or the use of liquid lenses[1,2]—approaches with high spatial occupancy and limited production scalability. Recently, optical metasurfaces composed of subwavelength-scale nanostructures (meta-atoms) have provided an ultrathin and lightweight platform for modulating the spatial and spectral properties of electromagnetic fields, promising the extreme miniaturization and extended functionality of photonic devices.[3,4] Semiconductor-based metasurfaces utilizing low-profile (submicron-thick) constituent meta-atoms can deliver diffraction-limited focusing because of their low nonradiative losses and precisely engineered phase response of their building blocks.[5,6] However, most focusing metasurfaces (metalenses) have fixed focal lengths, limiting their potential applications.

Several approaches to modulating metalens properties have been experimentally demonstrated. One approach uses mechanical forces to deform metasurfaces embedded in stretchable substrates or to displace or rotate the metasurfaces themselves.[7−12] Alternatively, nonmechanical tuning mechanisms are potentially advantageous for low power consumption, high tuning speed, small footprint, and longer lifespan of the resulting optical devices. Such reconfigurable metalenses have been achieved by combining birefringent metasurfaces with polarization rotation,[13−15] as well as integrating metasurfaces with active materials such as graphene,[16] phase change materials,[17−20] and liquid crystals (LCs).[21−25] Among all tuning mechanisms, electrical actuation represents one of the most practical methods for integration with compact imagers and wearable displays. LC-embedded metasurfaces represent an especially attractive approach since LC molecules possess an optical anisotropy of the refractive index $\Delta n = n_e - n_o$ that is large, sensitive to low-amplitude external electric fields,[26] and well-studied in the context of LC displays. LC-metasurfaces have enabled a diversity of active metadevices, including electrically tunable resonators,[27−32] chromatic aberration correctors,[21] active color filters,[33] dynamic beam steerers,[34,35] reconfigurable anomalous refraction components,[36] and, recently, bifocal lenses, that can switch between two discrete focal lengths.[24,25] Despite progress in developing LC-driven metalenses and their considerable potential, several challenges remain. Many imaging applications require

Received: August 22, 2024
Revised: December 23, 2024
Accepted: December 23, 2024

continuously variable focus (varifocal) zoom;[37] however, experimental implementations of LC-metalenses with this capability have yet to be realized. Moreover, the design complexity of tunable metalenses usually scales with lens diameter, restricting the ease of multizone realizations; this issue is sometimes circumvented by designs using the Pancharatnam−Berry phase effect, at the expense of restrictions on the polarization of incident light.

Here, we apply amorphous silicon (aSi)-metasurfaces infiltrated with LCs to address the aforementioned challenges. A general LC-metalens design as well as validation procedure is established to inform the selection of meta-atom candidates that yield the desired metalens response at each LC state, characterized by the director angle θ of the LC molecules. Our procedure involves the generation of an extensive meta-atom library, followed by the down-selection of candidate meta-atoms satisfying judiciously chosen constraints on their optical responses (i.e., the phase and amplitude of the transmitted light) for several LC director angles. The feasibility of the approach is verified through the numerical design and experimental demonstration of an LC-metalens exhibiting continuous modulation of its focal length $f(V_0)$ by up to 18% in response to a peak-to-peak AC bias voltage of $0 < V_0 < 9.8$ V (±4.9 V). Next, we present the design of wide-aperture switchable bifocal LC-metalenses with vastly simplified computational and fabrication complexity. This new design paradigm is used to fabricate two ∼3 mm-diameter imaging metalenses, each comprising only five designer meta-atoms, that exhibit high-contrast electrically actuated switching between two specified focal planes. The ultrathin profile, voltage actuation, and versatile functionalities of LC-metalenses render them well-suited for applications requiring compact zoom optics.

RESULTS

Operation Principles of LC-Metalenses. The LC-metalens concept is illustrated in Figure 1. The device consists

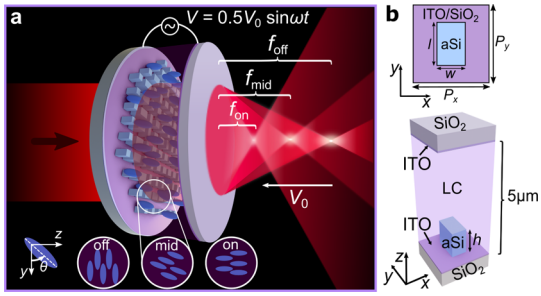

Figure 1. LC-embedded electrically actuated zoom metalenses. (a) Varifocal LC-metalens: the focal plane position behind the metalens is continuously varied between f_{off} and f_{on} as the ac voltage amplitude V_0 varies between $V_0 = V_{off}$ and $V_0 = V_{on}$. (b) Unit cell diagram: a periodic array of rectangular amorphous silicon meta-atoms embedded in an LC cell and sandwiched between ITO-coated silicon dioxide plates.

of a resonant metasurface embedded in a nematic LC and situated between two transparent conductive indium tin oxide (ITO) plates. The metasurface is engineered to impart a (hyperbolic) spatial phase profile onto the transmitted light that is sensitive to the orientation (director) angle θ of the surrounding LC molecules, such that in the absence of an external electric field, the LC alignment is in-plane and the metasuface focuses light at an initial focal length f_{off}. When an AC voltage $V(t) = 0.5V_0 \sin(2\pi ft)$ is applied across the LC cell (where $f = 1$ kHz, per industry standard, and V_0 denotes the signal's peak-to-peak voltage), LC molecules rotate out-of-plane and the focal length is tuned toward f_{on}. Depending on the design goal, the focal length may be continuously tuned between f_{off} and f_{on} as a function of V_0 (varifocal zoom lens) as shown in Figure 1a or discretely switched between f_{off} and f_{on} for two V_0 values (simplified bifocal imaging lens).

Metalens Design. The LC-metalens design procedure starts by defining two target phase maps corresponding to the $\theta = 0°$ ("off") and $\theta = 90°$ ("on") electrically controlled states of the LC. The off/on phase targets $\Phi_{off,on}(r, \lambda) \equiv \Phi(r, f = f_{off,on}, \lambda)$ follow a spatial phase profile of a converging lens:

$$\Phi(r, f(\theta), \lambda) = \frac{2\pi}{\lambda}\left(f - \sqrt{f^2 + r^2}\right) \quad (1)$$

where λ is the operation wavelength and r is the radial coordinate. For monochromatic metalenses discussed in this section, the dependence of $\Phi_{off,on}$ on λ will be made implicit for brevity. A Fresnel zone-type metalens design (detailed in 24) is utilized to approximate $\Phi(r, f \equiv f(\theta))$. In this scheme, the continuous phase profiles are discretized into a series of n concentric phase "zones", each providing phase delays in the $0 < \phi < 2\pi$ range. Each zone is further discretized into m equally spaced phase levels such that the phase delay of the jth phase level of (any) kth zone is given by $\phi_k^j(0°) = \frac{2\pi}{m}(j-1)$ for the "off-state". To approximate the spatial phase profile Φ_{off} in the "off-state", N_{off} meta-atoms with distinct geometries are selected to impart phases $\varphi^i(\theta = 0°) = \phi_k^j(0°)$ to the transmitted light at the target wavelength for $\theta = 0°$, where $0 < i < \mathcal{N}$ is the index of a meta-atom selected from a library of $\mathcal{N} \gg N_{off}$ meta-atom candidates (see below). Because of the finite size $\mathcal{N}$ of the library, the above expression can only be approximately satisfied: $\varphi^i(0°) \approx \phi_k^j(0°)$. Each of the N_{off} meta-atoms selected from the candidate library is placed at its corresponding radial position r_k^j. The expression for $r_k^j = \sqrt{\left(\frac{\lambda(\phi_k^j(0°) + 2\pi k)}{2\pi} + f_{off}\right)^2 - f_{off}^2}$ is obtained from eq 1 for the off-state of the LC: $\Phi_{off}(r_k^j) = \phi_k^j(0°)$. The selection of N_{off} meta-atoms constitutes the first down-selection step, as shown in Figure 2. Naturally, many meta-atom designs approximately satisfy the "off-state" condition. The challenge is to down-select this number to a much smaller set of meta-atom candidates that produce high-quality focusing in the "on-state", as well as the intermediate states.

To enable a monochromatic bifocal LC-metalens capable of voltage-actuated binary switching between two discrete focal planes at $z = f_{off}$ and $z = f_{on}$, the meta-atom geometries must be optimized to simultaneously impart phase delays of $\varphi^i(\theta = 90°) = \phi_k^j(90°) \equiv \Phi_{on}(r_k^j)$ corresponding to $\theta = 90°$ director angle of the LC. In general, $\Phi_{on}(r_k^j)$ depends on the zone number k. Therefore, we expect that the total number $N = m \cdot n < N_{off}$ of down-selected meta-atom geometries is needed to construct a tunable-focus metalens.

The selection of N unique meta-atom geometries satisfying the above constraints constitutes the second down-selection step depicted in Figure 2. As detailed in the following sections, imposing additional filters or performance figures of merits (FoMs) on the meta-atom library prior to the "off" and "on-state" down-selection steps can enable continuously variable

https://doi.org/10.1021/acsphotonics.4c01530
ACS Photonics XXXX, XXX, XXX−XXX

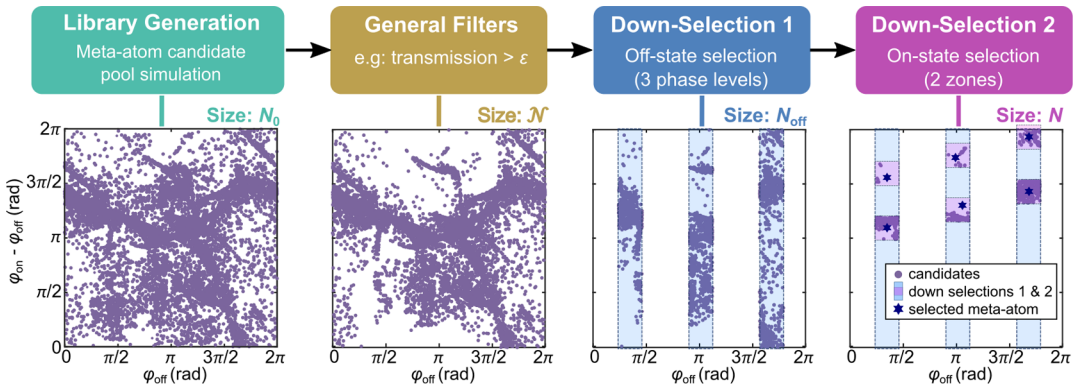

Figure 2. Basic workflow depicting the four-step optimization process for tunable-focus LC-metalenses. Step 1: Meta-atom library generation, following the procedure outlined in the main text. Step 2: Library candidates are omitted by predetermined filters, such as transmission or geometry requirements. Step 3: First down-selection step of meta-atoms, based on ϕ_{off} values, that enables focusing at $\theta = 0°$. Step 4: Second down-selection step of meta-atoms, based on ϕ_{on} values, enables a tunable-focus metalens. The shaded region serves to guide the eye. Its width (shown: 0.7 rad) is related to a user-defined error tolerance.

focal length as a function of V_0 or large numerical apertures. Below we detail how the library of meta-atom geometries is generated using electromagnetic simulations.

Meta-Atom Template and Library Generation. Amorphous silicon (aSi) was chosen as the constituent material of the metalens based on its low absorptive losses in the near-IR spectral window (see Figure S1 for aSi ellipsometry data) and established nanofabrication process. The metasurface unit cell—its meta-atom—consists of a rectangular aSi pillar situated on an ITO-coated fused silica substrate (Figure 1b). Periodic arrays of such semiconductor meta-atoms support localized electromagnetic Mie-type resonant optical modes, which are sensitive to the permittivity of the media adjacent to the array. Additionally, the rectangular meta-atom shape offers a relative ease of fabrication and up to three geometrical degrees of freedom for phase control. We note that the localized nature of metasurface resonances justifies using the assumption of an infinitely extended periodic array of meta-atoms, even though in reality, each meta-atom has a finite number of identical neighbors. The metasurface is infiltrated with a 5 μm-thick LC (E7 mixture by Merk[38]) and covered by a top ITO-coated silica plate. The 5 μm-thickness ensures that the LC cell extends well past the range influenced by the near-field effects of the metasurface. Planar prealignment of the LC molecules, which is approximately sustained across the full LC cell,[31] is achieved by mechanical brushing of a polymer atop the ITO coating of the top substrate. The ITO coatings function as top and bottom electrodes used to apply bias voltages across the LC cell. The LC can be modeled as a homogeneous anisotropic dielectric medium with $n_o = 1.51$, $n_e = 1.72$, and voltage-dependent director angle $\theta \equiv \theta(V_0)$ of the anisotropy axis as defined in Figure 1a. For the case of zero applied voltage, the initial alignment of LC molecules induced by the brushed top plate is in-plane with metasurface $\theta(V_0 = 0) = 0°$ along the y-axis Applying a nonzero voltage $V_0 > 0$ across the LC cell can rotate the molecular axis angle $\theta(V_0)$ by up to 90° in the $y - z$ plane, spectrally shifting the meta-atom resonances.

A pool of meta-atom candidates ($0 < i < N_0$) was generated in the 5D parameter space $[w, l, P, h, \theta]$ (see Figure 1b for geometry definitions) using-finite element-method COMSOL simulations under the assumption of normally incident light polarized along the y-axis (see Supporting Information Section S3). To simplify the simulation, a periodic square array was assumed, and the lattice constant $P = 475$ nm was chosen to avoid excitation of unwanted diffraction orders: $P < \lambda/n_e$. A set of equidistant LC director angles θ_q were chosen in the $0° \leq \theta \leq 90°$ range in increments of $\delta\theta = 22.5°$, i.e., $\theta_q = (q - 1)\delta\theta$ and $1 \leq q \leq 5$.

Active wavefront-shaping in the form of tunable lensing is contingent on the nontrivial realization of both a spatially varying parabolic phase-delay profile and LC-induced phase response that are locally customized at the meta-atom level, with complexity that scales with the number of targeted optical states. It is therefore essential that variations of the widths w and lengths l of the meta-atom pillars allow variable imparted phases spanning the full $0-2\pi$ range at two or more discrete LC orientations while maintaining acceptable transmission efficiencies above ϵ. We determined that a uniform height of $h = 300$ nm for all individual meta-atoms effectively balances this design requirement and fabrication viability. An efficiency filter is imposed on the meta-atom library (during step 2 in Figure 2) to ensure all meta-atom candidates provide $|t^i(\theta_q)|^2 > \epsilon$, where $t^i(\theta_q) \equiv |t^i| e^{i\varphi^i(\theta_q)}$ denotes the complex-valued transmission amplitude of the ith meta-atom at the qth LC director angle.

Down-Selection of Meta-Atoms and Experimental Demonstration of a Varifocal LC-metalens. Two essential properties of varifocal zoom systems include the continuity and smoothness of tuning including, but not limited to, unidirectional modulation and the absence of abrupt jumps of the focal length $f(\theta)$. One way of ensuring smooth tuning is to require that meta-atoms comprising a varifocal metalens follow conditions of monotonic and uniformly increasing phase increment $\Delta\varphi_q^i \equiv \varphi^i(\theta_q) - \varphi^i(\theta_{q-1})$ as a function of θ.[24] This is equivalent to smooth voltage-controlled tuning, as we assume $\theta(V_0)$ to be a monotonic function as a function of the voltage amplitude V_0. Thus, we select the meta-atoms satisfying the following conditions:

$$\varphi^i(\theta_5) < \varphi^i(\theta_4) < \varphi^i(\theta_3) < \varphi^i(\theta_2) < \varphi^i(\theta_1) \tag{2}$$

and

$$\zeta_q \equiv |\Delta\varphi_q^i| - |\Delta\varphi_{q-1}^i| < \zeta \tag{3}$$

https://doi.org/10.1021/acsphotonics.4c01530
ACS Photonics XXXX, XXX, XXX−XXX

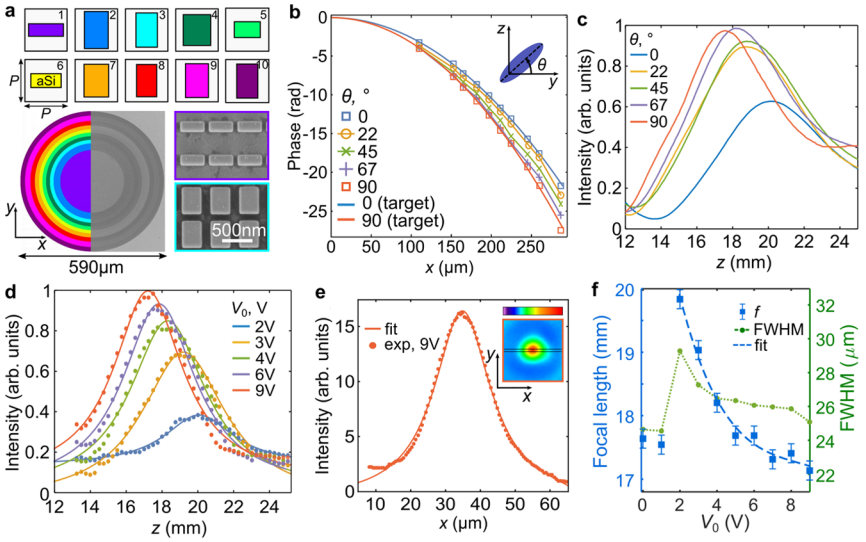

Figure 3. Design and experimental realization of an LC-metalens with continuously tunable focal length. (a) SEMs of the fabricated varifocal metalens. The different colors of the metalens correspond to its ten unique meta-atom geometries. For geometric parameters, see Table S1. (b) Simulated LC-angle-dependent phase distribution imparted by the selected meta-atoms as a function of the radial coordinate. Solid lines: the targeted phase functions of converging lenses with f_{off} = 20 mm and f_{on} = 18 mm. (c) Simulated and (d) measured on-axis intensities of the metalens along the optical axis z. (e) Normalized y-averaged (see the dashed rectangle in the inset) intensity $I(x, y \approx 0)$ in the "on" focal plane for the peak-to-peak voltage $V_0 = V_{on}$. Inset: Intensity profile of the focal spot in the xy-plane. Dashed rectangle: y-averaging area used for calculating $I(x, y \approx 0)$. Off (on) states: V_{off} = 2 V (V_{on} = 9 V). (f) Measured focal length f and fwhm of the focal spot as a function of V_0. Dashed blue lines serve to guide the eye. Error bars represent a ± 0.15 mm uncertainty arising from the estimated experimental in-focus (z = 0 mm) z-coordinate. Operation wavelength: λ = 808 nm.

where $\zeta \leq 2.5$ rad and $q \in [2, 5]$. Imposing these two varifocal conditions $\forall\ i$ down-filters the meta-atom library to include only those suitable for high-performance varifocal tuning between the "off" and "on"-states of the electrically tunable LC. Details of the varifocal metalens design proposed here and its advancements from our earlier numerical demonstration[24] are described in Supporting Information Section S9.

For the experimental proof-of-concept demonstration of a near-infrared varifocal metalens operating at λ = 808 nm, the optimization routine is applied to construct a metalens with n = 3 zones and m = 3 phase levels that gradually changes its focal plane location from $z = f_{off}$ = 20 mm to $z = f_{on}$ = 17 mm. The varifocal optimization involves a trade-off between effective library filtering and the preservation of low phase errors. We have determined that the varifocal constraint (eq 3) with $\zeta \leq 2.5$ rad is sufficient for ensuring a reasonable candidate library density while maintaining effective varifocal behavior. Additional geometrical filters were imposed on the library to maximize the fabrication viability of the metalens. Specifically, unit cell filling factors, defined as $F = w_x w_y P^{-2}$, were limited to the range F = 0.25−0.5 for all down-selected candidates. The geometry filters, varifocal filters (eqs 2 and 3), and the "off/on"-state phase targets were simultaneously met by N = 10 unique geometries of the down-selected meta-atoms.

Based on this design, a D = 0.59 mm-diameter metalens was fabricated using standard electron beam lithography (EBL) and reactive ion etching procedures; for details, see Supporting Information Section S2. Scanning electron microscopy (SEM) images of the fabricated metalens are displayed in Figure 3a, color-coded according to the individual meta-atom geometries and showing high-fidelity patterning consistent with the design parameters.

The simulated phases of the selected meta-atoms as a function of their radial position r^i and imparted phase φ^i are plotted in Figure 3b for the five values θ_q of the LC director angle. The results display close agreement with the targeted "off-state" and "on-state" continuous phase profiles as well as uniform and continuous phase modulation of each meta-atom for the intermediate LC orientations. The intensity of light along the optical axis z of the metalens, calculated using full-aperture COMSOL simulations and the Fraunhofer integral method (see Supporting Information Section S4 for details), reveals distinct intensity maxima for each value of θ, as shown in Figure 3c.

The varifocal performance of the fabricated metalens was characterized using a y-polarized laser diode as a monochromatic light source at λ = 808 nm and a complementary metal-oxide semiconductor camera to image the infrared light transmitted through the metalens (details in Supporting Information Figure S2). The distance z between the imaged xy-planes and the metalens was varied by translating the latter along the optical axis. The AC bias voltage across the LC cell was supplied by a function generator (details in Supporting Information Section S6). The resulting measured on-axis intensity of the metalens is presented in Figure 3d, showing continuous and high-contrast tuning of the focal plane between z = 20 mm and z = 17 mm as the peak-to-peak AC voltage applied across the LC cell is gradually increased from $V_0 = V_{off}$ to $V_0 = V_{on}$, in excellent agreement with the simulated results. Measured voltage-dependent cross-sectional intensity profiles of the varifocal LC-metalens in the xz-plane are presented in Figure S5. A representative 2D focal plane intensity profile $I(x, y, z = f_{on})$ measured for $V_0 = V_{on}$ is shown in Figure 3e in the "on-state" (see the inset), as well as its lineout $\overline{I}_{on}(x) \equiv \langle I(x, y = 0, z = f_{on}) \rangle$ along the x-axis (dotted curve). The experimentally measured $\overline{I}_{on}(x)$ is well-fitted to a Gaussian

https://doi.org/10.1021/acsphotonics.4c01530
ACS Photonics XXXX, XXX, XXX−XXX

line shape (solid line), indicating that the focused beam is indeed Gaussian in the "on-state". For several other values of applied voltages, similar Gaussian line shape fits of the measured intensity lineouts in their corresponding focal planes $z = f(V_0)$ were used to extract the full width at half-maxima (fwhm) $w(V_0)$. The extracted focal length $f(V_0)$ (blue dashed line) and fwhm $w(V_0)$ (green dotted line) of the metalens are plotted in Figure 3f as a function of the applied voltage. Our experiments indicate the threshold voltage of the LC cell is near $V_{th} = 2$ V, with the LC molecule and subsequent varifocal performance achieved for applied voltages above this threshold, i.e., $V_{off} \equiv V_{th} \leq V_0 \leq V_{on}$. A smooth monotonic decrease of f accompanied by a near-diffraction-limited fwhm is observed over the full range of voltages. We have found that the Strehl ratios vary between $S_{off} \approx 0.47$ and $S_{on} \approx 0.61$ for all values of V_0 (see Figure S3), close to the theoretical limit of ~0.68 for a three-phase-level lens.[39,40]

On the other hand, the focusing efficiencies were found to vary between $\eta_{off} = 8.2\%$ and $\eta_{on} = 11.8\%$, indicating that additional design improvements may be needed to increase the amount of transmitted light. For the presented proof-of-principle LC-metalens, several intentional design choices aimed at easing meta-atom fabrication complexity (e.g., small filling-factors F and minimum periodicity P) and restricting the meta-atom shapes to simple low-profile rectangular pillars limited the efficiency of our demonstration device. Moreover, although the metalens uses only $m = 3$ discrete phase levels per Fresnel zone (to ensure modest fabrication complexity), the focusing efficiency could be further raised by utilizing an eight-level scheme.[39]

A second varifocal metalens was fabricated with an identical pattern and process conditions as the one presented in Figure 3. Its characterization (Figure S4a) shows a comparable tuning range and Strehl ratios to those shown in Figure 3. We have also verified that the measured focal length is not monotonically responding to applied voltage and does not have the same overall tuning range when incident light is orthogonally polarized or has the incorrect operation wavelength $\lambda = 690$ nm (Figure S4b,c), as indeed expected from a metalens based on anisotropic resonant meta-atoms.

Simplified Design of Wide-Aperture Bifocal Metalenses. Wide-diameter lenses are of substantial interest to various imaging technologies,[41] as the immediate consequence of the Abbe resolution limit $\Delta \sim \lambda/2$ NA, where Δ and NA are the spatial resolution and numerical aperture ($NA \approx D/2f$) of a lens, respectively. However, the selection of meta-atom candidates fulfilling the phase criteria for large-diameter varifocal metalenses poses a significant optimization challenge: each additional Fresnel zone subdivided into m phase levels generally requires m distinct phase targets $\phi_k^i(\theta = 90°)$ and, therefore, the same number of unique meta-atom candidates. Mathematically, the total number of zones n approximately scales quadratically with diameter: $n \approx \frac{D^2}{8\lambda f}$. For example, a $D =$ 2 mm-wide four-level lens with $f_{off} = 13$ mm, $f_{on} = 11$ mm, $\lambda_0 =$ 808 nm, and $P_x = P_y = 470$ nm would require $n \sim 45$ Fresnel zones and therefore more than $m \cdot n = 190$ different meta-atom geometries. In practice, the feasibility of selecting and fabricating hundreds of unique meta-atom geometries is limited by the finite size $\mathcal{N}$ of the meta-atom library and EBL optimization complexity, respectively. To address this challenge, we introduce a general relationship between f_{off} and f_{on} of a Fresnel-type bifocal lens such that each new zone added to the metalens utilizes exactly the same set of phase targets and associated meta-atom unit cells as one of the previous zones. Such bifocal LC-metalenses are suitable for a subset of imaging applications that require discrete imaging operations.[42,43]

Under the simplifying assumptions of the paraxial limit and $f_{on}/f_{off} = a/m$, where a is an integer and m is the number of phase levels per Fresnel zone in the "off"-state, the following relation holds for the minimal number M of meta-atom geometries needed to construct a bifocal lens with any diameter (i.e., regardless of the number of Fresnel zones):

$$M = \frac{am}{\mathrm{GCF}(a, m)} \equiv mp_s \tag{4}$$

where $\mathrm{GCF}(p, q)$ is the greatest common factor of two integers, p and q, and p_s is a superperiod as explained below. The derivation is provided in Supporting Information Section S10. Naturally, m and a have to be judiciously chosen to satisfy the simplifying focal length ratio condition. Consider a simple example: $f_{on} = f_{off}/R$, where R is an integer number. Then, by choosing m to be a multiple of R and $a = m/R$, we obtain $M = m$ from eq 4, i.e., the superperiod $p_s = 1$ and all meta-atom geometries from the first Fresnel zone can be recycled for every subsequent zone. Another example illustrating the case of $p_s \neq 1$ is $f_{on} = 2f_{off}/3$. By choosing $m = 6$ and $a = 4$, we obtain $M = 12$ or $p_s = 2$. Therefore, the meta-atom geometries used in $n = 1$ and $n = 2$ Fresnel zones can be reused in all of the subsequent zones starting from $n = 3$. Maximum diameter limits as well as a method to enable $f_{off} > f_{on}$ with $M = m$ are discussed in Supporting Information Section S10.

Below, we validate the concept of a simplified bifocal metalens by designing two high-performance LC-metalenses that change their focal distances from f_{off} to $f_{on} = f_{off}/2$ (Type-I, hereafter) or to $f_{on} = -f_{off}$ (Type-II). Only $M = m = 5$ meta-atoms are needed because of the integer relationship between the focal distances f_{on} and f_{off}. As in the example of the varifocal lens, these focal plane shifts are accomplished by changing the orientation of the LC molecules from $\theta = 0°$ to $\theta = 90°$. Although metalens designs leveraging the PB phase effect can also significantly simplify the number of unique meta-atoms required per bifocal metalens by utilizing in-plane meta-atom rotation as an additional degree of freedom, the derivation of eq 4 is free of any stipulations on the incident polarization of light or the introduction of additional polarizing elements, which are typical prerequisites of the PB phase method.[17,25] Notably, polarization insensitivity could broaden the applicability of LC-metalenses by enabling compatibility with various light sources and by eliminating the need for device alignment with the incident beam's polarization axis. Although our designs utilize polarization-sensitive resonances, we envision achieving polarization-insensitive bifocal LC-metalenses through modifications to the meta-atom shapes and LC prealignment. For instance, rotationally symmetric meta-atoms, such as annular cylinders, combined with an isotropic LC "off-state", could lead to polarization-insensitive bifocal metalenses.

Experimental Realization of Simplified Wide-Aperture Bifocal LC-Metalenses. Two devices were fabricated for experimental verification: a Type-I bifocal lens with $m = 5$, $D = 2.8$ mm, $f_{off} = 22$ mm, and $f_{on} = 11$ mm, and a Type-II bifocal lens with $m = 3$, $D = 2.9$ mm, $f_{off} = +9$ mm, and $f_{on} = -9$ mm. The resulting Type-I and Type-II lenses are composed of $n = 55$ and $n = 140$ zones, respectively. Color-coded SEM images of the $M = 5$ meta-atom geometries for the Type-I

https://doi.org/10.1021/acsphotonics.4c01530
ACS Photonics XXXX, XXX, XXX−XXX

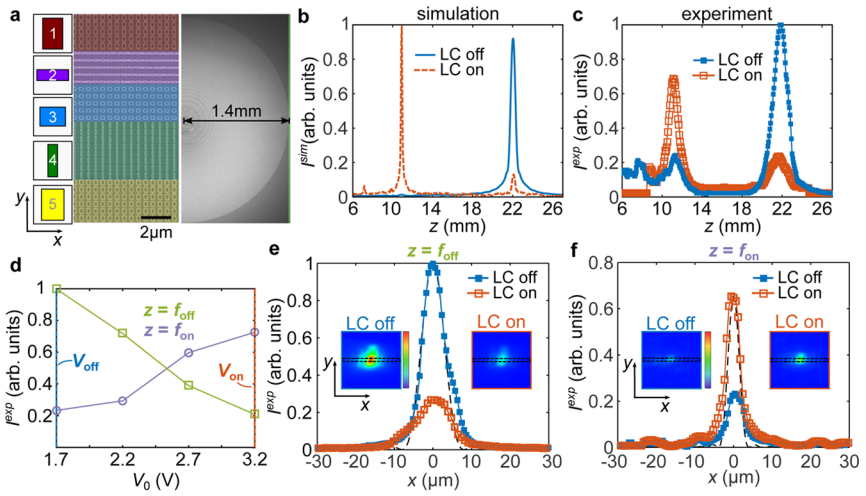

Figure 4. Demonstration of LC-driven wide-aperture bifocal metalenses. (a) SEM images of the fabricated metalens, shaded according to its $m = 5$ phase levels. (b) Simulated intensity along the optical axis (z) of the designed metalens for "off" (blue solid line) and "on" (orange dashed line) LC states, calculated using the Fourier-propagation method detailed in Supporting Information Section S4. (c) Measured on-axis intensity of the fabricated metalens for "off" (blue solid squares) and "on" (orange squares) LC states. (d) Focal spot intensities at $z = f_{off}$ and $z = f_{on}$ plotted as a function of peak-to-peak voltage V_0. (e,f) Averaged cross-sectional intensity of the focal spot images at $V_0 = 1.7$ V ("off-state") and $V_0 = 3.2$ V ("on-state") for (e) $z = f_{off}$ and (f) $z = f_{on}$. Insets show the respective beam profiles of the focal spots in the "off"/"on"-states, with dashed rectangles indicating the y-averaging areas. Parameters: $f_{on} = f_{off}/2 = 11$ mm.

metalens are shown in Figure 4a. Note that a transmission constraint of $|t_i(\theta_{off,on})|^2 > 0.35$ was imposed on the meta-atom library.

The calculated intensity transmitted through the fabricated metalens (Figure 4b) shows pronounced high-contrast maxima at the designed focal planes corresponding to the off/on-states. The experimental results for Type-I LC-metalens are in good agreement with our theoretical calculations, as shown in Figure 4c. Figure 4d plots the peak intensities of the two focal spots as a function of V_0, showing a gradual monotonic redistribution of energy between the two focal spots as V_0 is increased in the range $V_{off} \le V_0 \le V_{on}$, where $V_{off} = 1.7$ V and $V_{on} = 3.2$ V. The optical intensity profiles across the focal planes are plotted in Figure 4e,f, and the correlated 2D focal spot images are shown in the insets. As the applied voltages are toggled between the $V_0 = V_{off}$ and $V_0 = V_{on}$ values, the focal spot dims in the $z = f_{off}$ focal plane, as seen in Figure 4e. The opposite effect is observed at $z = f_{on}$, as shown in Figure 4f. The discrepancies between experimental and theoretical switching contrast are attributed to the phase disorder introduced by fabrication imperfections. Such imperfections may include nonideal meta-atom geometries, refractive indices, and LC alignment. By switching from the off to the on voltage, the peak focal spot intensity at $z = f_{off}$ decreases by 75% and the focal spot intensity at $z = f_{on}$ increases by 47%. The high switching contrast in the focal planes and the negligible intensity elsewhere indicate good prospects for imaging at multiple focal planes without significant cross-talk between the two. The Strehl ratios of the focal spots in the off- and on-states of the LC are 0.77 and 0.54, respectively, indicating the near-diffraction-limited performance of the device in the "off-state", and the corresponding focusing efficiencies are 0.41 and 0.34.

Analogous toggling of the Type-II metalens between convergent ($f_{off} = +9$ mm) and divergent ($f_{on} = -9$ mm) states is observed, and the results are presented in Figure S8. Although a maximum NA of 0.17 was targeted for both experimental demonstrations, in principle, a wide range of diameters and corresponding NAs is accessible by the proposed metalens design based on $N = 5$ unique geometries.

Imaging with Wide-Aperture Bifocal LC-Metalenses. The dynamic imaging capabilities of the fabricated bifocal lenses were demonstrated by using a 1951 United States Air Force (USAF) resolution target. For brevity, Figure 5 summarizes the imaging data of the fabricated Type-I bifocal metalens, whereas the Type-II bifocal metalens imaging results are shown in Supporting Information Section S7. The optical configuration shown in Figure 5e was used to image USAF target Group 3 Elements 4–6 (minimum feature size: 35 μm) in the two LC-switchable imaging planes of the metalens. The object distance, $o = 44$ mm, was chosen to produce sharp images of the target in both LC states (see Supporting Information Section S6 for details). The relation between the object and image distances is given by

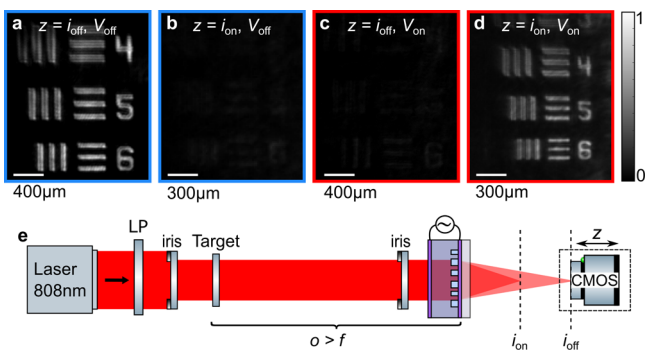

Figure 5. Electrically actuated imaging using a wide-aperture bifocal LC-metalens. Images of a negative USAF resolution target formed in the imaging planes of the metalens in the (a, c) $f = f_{off}$ and (b, d) $f = f_{on}$ states, recorded for the "off" and "on" voltages. (e) Schematic of the optical setup to image the negative resolution target with a Type-I bifocal metalens. Parameters: $V_{off} = 1.7$ V, $V_{on} = 3.2$ V, $f_{off} = 22$ mm, $f_{on} = f_{off}/2 = 11$ mm.

https://doi.org/10.1021/acsphotonics.4c01530
ACS Photonics XXXX, XXX, XXX−XXX

$$1/o + 1/i_{\mathrm{off,on}} = 1/f_{\mathrm{off,on}} \quad (5)$$

where o and $i_{\mathrm{off,on}}$ are the object and image distances relative to the metalens, respectively (defined in Figure 5e). A bright, clearly resolved image appears in the $z = i_{\mathrm{off}}$ plane for $V_0 = V_{\mathrm{off}}$ (Figure 5a), while the $z = i_{\mathrm{on}}$ image plane is dark for the same voltage (Figure 5b). By increasing the voltage from $V_0 = V_{\mathrm{off}}$ to $V_0 = V_{\mathrm{on}}$, active switching between the two imaging planes is demonstrated: the well-resolved image in the $z = i_{\mathrm{off}}$ plane becomes dim and indistinct (Figure 5c), while the image in the $z = i_{\mathrm{on}}$ plane becomes brighter and in-focus (Figure 5d). As expected, the "off-" and "on-state" focal lengths, calculated using eq 5 and the experimental o, i values, were consistent with the metalens design (details in Supporting Information Section S6). The maximum spatial frequency of the imaged Group 3 elements is much less than the cutoff frequency of the metalens; subsequently, to test the limits of the metalens resolving power, the highest-resolvable frequency group of the USAF target by the metalens was investigated and determined to be Group 6, element 1 (image shown in Figure S7) with 7.8 μm line widths, in agreement with the characterized fwhm of the focal spots (Figure 4f), and 1.2 times larger than the theoretical Rayleigh resolution limit of the metalens: ~6.4 μm in the "on-state" for the designed NA = 0.13.

OUTLOOK AND CONCLUSIONS

While the focusing efficiency of the LC-metalenses presented in this work ranges from 0.08 to 0.41, the efficiency and tuning contrast of the devices can be raised with increased structural complexity of meta-atoms and the number of discrete phase levels per Fresnel zone. Efficient metalens design may also benefit from recent developments in deep-learning-based design algorithms.[44,45] Moreover, although our nematic-LC-based numerical models already closely predict the experimental results, we note that metalens performance depends sensitively on the LC molecules' proper alignment and anchoring. Therefore, enhanced experimental mitigation and computational modeling of LC alignment inhomogeneities[46−50] could significantly assist future LC-metalenses. Finally, our design method is readily generalized to other spectral ranges by an appropriate choice of meta-atom materials with low absorptive loss, opening possibilities for LC-driven red-green-blue zoom components: a topic of future work.

To conclude, we have demonstrated multifunctional flat lenses with electrically actuated zoom based on LC-encapsulated resonant semiconductor metasurfaces. The design approach utilizes the strong electro-optical response of LCs to electrically tune the meta-atom resonances, yielding considerable real-time modulations to the spatial phase profile of transmitted light. The phase accumulation and modulation are uncoupled from the LC cell thickness, therefore enabling zoom lenses to rival the performance of traditional LC-only tunable lenses while being only a fraction of the thickness.[2,51] Our numerical simulations verify several LC-metalens designs with distinct functions, including electrically driven varifocal zoom and simplified wide-aperture imaging. We experimentally demonstrate a voltage-driven LC-metalens with a continuously tunable focal length from 20 to 17 mm, as well as simplified millimeter-scale LC-metalenses that facilitate electrically switchable imaging between two focal planes simultaneously with a drastic reduction in computation cost and fabrication complexity. Our results represent a key demonstration of ultrathin voltage-tunable multifunctional zoom lenses of interest to various imaging technologies such as light detection and ranging and wearable displays.

ASSOCIATED CONTENT

Data Availability Statement

Data that support the findings of this study are available within the main text and the Supporting Information.

Supporting Information

The Supporting Information is available free of charge at https://pubs.acs.org/doi/10.1021/acsphotonics.4c01530.

Detailed sample fabrication, numerical simulations, and optimization of meta-atom candidates; ellipsometry of aSi films; derivation of simplified bifocal metalens conditions; description of optical measurements; and experimental evaluation of additional varifocal and Type-II bifocal devices (PDF)

AUTHOR INFORMATION

Corresponding Authors

Melissa Bosch − *Department of Physics, Cornell University, Ithaca, New York 14853, United States;* orcid.org/0009-0009-2296-2749; Email: mb2583@cornell.edu

Gennady Shvets − *School of Applied and Engineering Physics, Cornell University, Ithaca, New York 14853, United States;* Email: gshvets@cornell.edu

Authors

Maxim Shcherbakov − *Department of Electrical Engineering and Computer Science, University of California, Irvine, California 92697, United States;* orcid.org/0000-0001-7198-5482

Kanghee Won − *Department of Information Display, Kyung Hee University, Dongdaemun-gu Seoul 02447, South Korea*

Hong-Seok Lee − *Major of Electrical Engineering, College of Engineering, Pukyong National University, Busan 48513, South Korea;* orcid.org/0000-0002-3081-7666

Young Kim − *Samsung Advanced Institute of Technology (SAIT), Samsung Electronics, Co. Ltd., Suwon-si, Gyeonggi-do 16678, South Korea*

Complete contact information is available at: https://pubs.acs.org/10.1021/acsphotonics.4c01530

Funding

This work was supported by the Office of Naval Research (ONR) Award No. N00014−21−1−2056 and the Global Research Outreach program of Samsung Advanced Institute of Technology. This work was performed in part at the Cornell NanoScale Science and Technology Facility (CNF), a member of the National Nanotechnology Coordinated Infrastructure (NNCI), which is supported by the National Science Foundation (Grant No. NNCI-2025233).

Notes

The authors declare no competing financial interest.

ACKNOWLEDGMENTS

This paper is adapted from the PhD dissertation of Melissa Bosch, completed in 2024 at the Department of Physics, Cornell University.

REFERENCES

(1) Blum, M.; Büeler, M.; Grätzel, C.; Aschwanden, M. Compact Optical Design Solutions using Focus Tunable Lenses. *Opt. Des. Eng. IV* **2011**, *8167*, 81670W.

(2) Lin, H.-C.; Chen, M.-S.; Lin, Y.-H. A Review of Electrically Tunable Focusing Liquid Crystal Lenses. *Transactions on Electrical and Electronic Materials* **2011**, *12*, 234−240.

(3) Holloway, C. L.; Kuester, E. F.; Gordon, J. A.; O'Hara, J.; Booth, J.; Smith, D. R. An Overview of the Theory and Applications of Metasurfaces: The Two-Dimensional Equivalents of Metamaterials. *IEEE Antennas and Propagation Magazine* **2012**, *54*, 10−35.

(4) Yu, N.; Capasso, F. Flat Optics with Designer Metasurfaces. *Nat. Mater.* **2014**, *13*, 139−150.

(5) Genevet, P.; Capasso, F.; Aieta, F.; Khorasaninejad, M.; Devlin, R. Recent Advances in Planar Optics: From Plasmonic to Dielectric Metasurfaces. *Optica* **2017**, *4*, 139−152.

(6) Wang, Y.; Chen, Q.; Yang, W.; Ji, Z.; Jin, L.; Ma, X.; Song, Q.; Boltasseva, A.; Han, J.; Shalaev, V. M.; et al. High-efficiency Broadband Achromatic metalens for Near-IR Biological Imaging Window. *Nat. Commun.* **2021**, *12*, 5560.

(7) Ee, H. S.; Agarwal, R. Tunable Metasurface and Flat Optical Zoom Lens on a Stretchable Substrate. *Nano Lett.* **2016**, *16*, 2818−2823.

(8) Arbabi, E.; Arbabi, A.; Kamali, S. M.; Horie, Y.; Faraji-Dana, M. S.; Faraon, A. MEMS-tunable Dielectric Metasurface Lens. *Nat. Commun.* **2018**, *9*, 812.

(9) Han, Z.; Colburn, S.; Majumdar, A.; Böhringer, K. F. MEMS-actuated Metasurface Alvarez Lens. *Microsyst. Nanoeng.* **2020**, *6*, 79.

(10) Meng, C.; Thrane, P. C.; Ding, F.; Gjessing, J.; Thomaschewski, M.; Wu, C.; Dirdal, C.; Bozhevolnyi, S. I. Dynamic Piezoelectric MEMS-based Optical Metasurfaces. *Sci. Adv.* **2021**, *7*, No. eabg5639.

(11) Luo, Y.; Chu, C. H.; Vyas, S.; Kuo, H. Y.; Chia, Y. H.; Chen, M. K.; Shi, X.; Tanaka, T.; Misawa, H.; Huang, Y.-Y.; et al. Varifocal metalens for Optical Sectioning Fluorescence Microscopy. *Nano Lett.* **2021**, *21*, 5133−5142.

(12) Colburn, S.; Zhan, A.; Majumdar, A. Varifocal Zoom Imaging with Large Area Focal Length Adjustable Metalenses. *Optica* **2018**, *5*, 825−831.

(13) Aiello, M. D.; Backer, A. S.; Sapon, A. J.; Smits, J.; Perreault, J. D.; Llull, P.; Acosta, V. M. Achromatic Varifocal metalens for the Visible Spectrum. *ACS Photonics* **2019**, *6*, 2432−2440.

(14) Liu, M.; Zhu, W.; Huo, P.; Feng, L.; Song, M.; Zhang, C.; Chen, L.; Lezec, H. J.; Lu, Y.; Agrawal, A.; et al. Multifunctional Metasurfaces Enabled by Simultaneous and Independent Control of Phase and Amplitude for Orthogonal Polarization States. *Light: Sci. Appl.* **2021**, *10*, 107.

(15) Huang, P.-S.; Chu, C. H.; Huang, S.-H.; Su, H.-P.; Tanaka, T.; Wu, P. C. Varifocal Mtalenses: Harnessing Polarization-dependent Superposition for Continuous Focal Length Control. *Nano Lett.* **2023**, *23*, 10432−10440.

(16) Ding, P.; Li, Y.; Shao, L.; Tian, X.; Wang, J.; Fan, C. Graphene Aperture-based metalens for Dynamic Focusing of Terahertz Waves. *Opt. Express* **2018**, *26*, 28038.

(17) Shalaginov, M. Y.; An, S.; Zhang, Y.; Yang, F.; Su, P.; Liberman, V.; Chou, J. B.; Roberts, C. M.; Kang, M.; Rios, C.; et al. Reconfigurable All-Dielectric metalens with Diffraction-limited Performance. *Nat. Commun.* **2021**, *12*, 1225.

(18) Zhang, Y.; Li, Z.; Qin, S.; Huang, H.; Jie, K.; Guo, J.; Liu, H.; Meng, H.; Wang, F.; Yang, X.; et al. Band-tunable Achromatic metalens based on Phase Change Material. *Opt. Express* **2022**, *30*, 17541−17553.

(19) Badloe, T.; Kim, I.; Rho, J. Moth-eye Shaped On-demand Broadband and Switchable Perfect Absorbers Based on Vanadium Dioxide. *Sci. Rep.* **2020**, *10*, 4522.

(20) Yang, F.; Lin, H.-I.; Shalaginov, M. Y.; Stoll, K.; An, S.; Rivero-Baleine, C.; Kang, M.; Agarwal, A.; Richardson, K.; Zhang, H.; et al. Reconfigurable Parfocal Zoom metalens. *Adv. Opt. Mater.* **2022**, *10*, No. 2200721.

(21) Shen, Z.; Zhou, S.; Li, X.; Ge, S.; Chen, P.; Hu, W.; Lu, Y. Liquid Crystal Integrated metalens with Tunable Chromatic Aberration. *Adv. Photonics* **2020**, *2*, No. 036002.

(22) Zhou, S.; Shen, Z.; Li, X.; Ge, S.; Lu, Y.; Hu, W. Liquid Crystal Integrated metalens with Dynamic Focusing Property. *Opt. Lett.* **2020**, *45*, 4324−4327.

(23) Hu, Y.; Ou, X.; Zeng, T.; Lai, J.; Zhang, J.; Li, X.; Luo, X.; Li, L.; Fan, F.; Duan, H. Electrically Tunable Multifunctional Polarization-dependent Metasurfaces Integrated with Liquid Crystals in the Visible Region. *Nano Lett.* **2021**, *21*, 4554−4562.

(24) Bosch, M.; Shcherbakov, M. R.; Won, K.; Lee, H.-S.; Kim, Y.; Shvets, G. Electrically Actuated Varifocal Lens based on Liquid-crystal-embedded Dielectric Metasurfaces. *Nano Lett.* **2021**, *21*, 3849−3856.

(25) Badloe, T.; Kim, I.; Kim, Y.; Kim, J.; Rho, J. Electrically Tunable Bifocal metalens with Diffraction-Limited Focusing and Imaging at Visible Wavelengths. *Adv. Sci.* **2021**, *8*, No. 2102646.

(26) Blinov, L. M. *Structure and Properties of Liquid Crystals*; Springer Science & Business Media, 2010; Vol. *123*.

(27) Gorkunov, M. V.; Osipov, M. A. Tunability of Wire-grid Metamaterial Immersed into Nematic Liquid Crystal. *J. Appl. Phys.* **2008**, *103*, No. 036101.

(28) Xiao, S.; Chettiar, U. K.; Kildishev, A. V.; Drachev, V.; Khoo, I. C.; Shalaev, V. M. Tunable Magnetic Response of Metamaterials. *Appl. Phys. Lett.* **2009**, *95*, No. 033115.

(29) Buchnev, O.; Ou, J. Y.; Kaczmarek, M.; Zheludev, N. I.; Fedotov, V. A. Electro-optical Control in a Plasmonic Metamaterial Hybridised with a Liquid-crystal Cell. *Opt. Express* **2013**, *21*, 1633.

(30) Decker, M.; Kremers, C.; Minovich, A.; Staude, I.; Miroshnichenko, A. E.; Chigrin, D.; Neshev, D. N.; Jagadish, C.; Kivshar, Y. S. Electro-optical Switching by Liquid-crystal Controlled Metasurfaces. *Opt. Express* **2013**, *21*, 8879−8885.

(31) Komar, A.; Fang, Z.; Bohn, J.; Sautter, J.; Decker, M.; Miroshnichenko, A.; Pertsch, T.; Brener, I.; Kivshar, Y. S.; Staude, I.; Neshev, D. N. Electrically Tunable All-Dielectric Optical Metasurfaces based on Liquid Crystals. *Appl. Phys. Lett.* **2017**, *110*, No. 071109.

(32) Parry, M.; Komar, A.; Hopkins, B.; Campione, S.; Liu, S.; Miroshnichenko, A. E.; Nogan, J.; Sinclair, M. B.; Brener, I.; Neshev, D. N. Active Tuning of High-Q Dielectric Metasurfaces. *Appl. Phys. Lett.* **2017**, *111*, No. 053102.

(33) Driencourt, L.; Federspiel, F.; Kazazis, D.; Tseng, L.-T.; Frantz, R.; Ekinci, Y.; Ferrini, R.; Gallinet, B. Electrically Tunable Multicolored Filter using Birefringent Plasmonic Resonators and Liquid Crystals. *Acs Photonics* **2020**, *7*, 444−453.

(34) Wu, J.; Shen, Z.; Ge, S.; Chen, B.; Shen, Z.; Wang, T.; Zhang, C.; Hu, W.; Fan, K.; Padilla, W.; et al. Liquid Crystal Programmable Metasurface for Terahertz Beam Steering. *Appl. Phys. Lett.* **2020**, *116*, 131104.

(35) Komar, A.; Paniagua-Dominguez, R.; Miroshnichenko, A.; Yu, Y. F.; Kivshar, Y. S.; Kuznetsov, A. I.; Neshev, D. Dynamic Beam Switching by Liquid Crystal Tunable Dielectric Metasurfaces. *ACS Photonics* **2018**, *5*, 1742−1748.

(36) Gorkunov, M. V.; Mamonova, A. V.; Kasyanova, I. V.; Ezhov, A. A.; Artemov, V. V.; Simdyankin, I. V.; Geivandov, A. R. Double-sided Liquid Crystal Metasurfaces for Electrically and Mechanically Controlled Broadband Visible Anomalous Refraction. *Nanophotonics* **2022**, *11*, 3901−3912.

(37) Kang, S.; Duocastella, M.; Arnold, C. B. Variable Optical Elements for Fast Focus Control. *Nat. Photonics* **2020**, *14*, 533−542.

(38) Li, J.; Wu, S.-T.; Brugioni, S.; Meucci, R.; Faetti, S. Infrared Refractive Indices of Liquid Crystals. *J. Appl. Phys.* **2005**, *97*, No. 073501.

(39) Aieta, F.; Genevet, P.; Kats, M.; Capasso, F. Aberrations of Flat lenses and Aplanatic Metasurfaces. *Opt. Express* **2013**, *21*, 31530−31539.

(40) Pan, M.; Fu, Y.; Zheng, M.; Chen, H.; Zang, Y.; Duan, H.; Li, Q.; Qiu, M.; Hu, Y. Dielectric metalens for Miniaturized Imaging Systems: Progress and Challenges. *Light: Sci. Appl.* **2022**, *11*, 195.

https://doi.org/10.1021/acsphotonics.4c01530
ACS Photonics XXXX, XXX, XXX−XXX

(41) Lee, G.-Y.; Hong, J.-Y.; Hwang, S.; Moon, S.; Kang, H.; Jeon, S.; Kim, H.; Jeong, J.-H.; Lee, B. Metasurface Eyepiece for Augmented Reality. *Nat. Commun.* **2018**, *9*, 4562.
(42) Love, G. D.; Hoffman, D. M.; Hands, P. J.; Gao, J.; Kirby, A. K.; Banks, M. S. High-speed Switchable Lens Enables the Development of a Volumetric Stereoscopic Display. *Opt. Express* **2009**, *17*, 15716.
(43) Li, G.; Mathine, D. L.; Valley, P.; Äyräs, P.; Haddock, J. N.; Giridhar, M. S.; Williby, G.; Schwiegerling, J.; Meredith, G. R.; Kippelen, B.; Honkanen, S.; Peyghambarian, N. Switchable Electro-optic Diffractive Lens with High Efficiency for Ophthalmic Applications. *Proc. Natl. Acad. Sci. U.S.A.* **2006**, *103*, 6100−6104.
(44) So, S.; Badloe, T.; Noh, J.; Bravo-Abad, J.; Rho, J. Deep Learning Enabled Inverse Design in Nanophotonics. *Nanophotonics* **2020**, *9*, 1041−1057.
(45) Ma, W.; Liu, Z.; Kudyshev, Z. A.; Boltasseva, A.; Cai, W.; Liu, Y. Deep Learning for the Design of Photonic Structures. *Nat. Photonics* **2021**, *15*, 77−90.
(46) Sun, M.; Xu, X.; Sun, X. W.; Valuckas, V.; Zheng, Y.; Paniagua-Domínguez, R.; Kuznetsov, A. I.; et al. Efficient Visible Light Modulation based on Electrically Tunable All Dielectric Metasurfaces Embedded in Thin-layer Nematic Liquid Crystals. *Sci. Rep.* **2019**, *9*, 8673.
(47) Dolan, J. A.; Cai, H.; Delalande, L.; Li, X.; Martinson, A. B.; de Pablo, J. J.; Lopez, D.; Nealey, P. F. Broadband Liquid Crystal Tunable Metasurfaces in the Visible: Liquid Crystal Inhomogeneities Across the Metasurface Parameter Space. *ACS Photonics* **2021**, *8*, 567−575.
(48) Lininger, A.; Zhu, A. Y.; Park, J.-S.; Palermo, G.; Chatterjee, S.; Boyd, J.; Capasso, F.; Strangi, G. Optical Properties of Metasurfaces Infiltrated with Liquid Crystals. *Proc. Natl. Acad. Sci. U. S. A.* **2020**, *117*, 20390−20396.
(49) Sautter, J.; Staude, I.; Decker, M.; Rusak, E.; Neshev, D. N.; Brener, I.; Kivshar, Y. S. Active Tuning of All-Dielectric Metasurfaces. *ACS Nano* **2015**, *9*, 4308−4315.
(50) Maruthiyodan Veetil, R.; Xu, X.; Dontabhaktuni, J.; Liang, X.; Kuznetsov, A. I.; Paniagua-Dominguez, R. Nanoantenna Induced Liquid Crystal Alignment for High Performance Tunable Metasurface. *Nanophotonics* **2024**, *13*, 2127−2139.
(51) Li, L.; Bryant, D.; Van Heugten, T.; Bos, P. J. Physical Limitations and Fundamental Factors Affecting Performance of Liquid Crystal Tunable Lenses with Concentric Electrode Rings. *Appl. Opt.* **2013**, *52*, 1978−1986.

https://doi.org/10.1021/acsphotonics.4c01530
ACS Photonics XXXX, XXX, XXX−XXX